J|A|C|S ARTICLES

Published on Web 03/12/2010

Anion-Vacancy-Induced Magneto−Crystalline Anisotropy in Fluorine-Doped Hexagonal Cobaltites

Olivier Mentré,[†] Houria Kabbour,*[,†] Ghislaine Ehora,[†] Grégory Tricot,[†] Sylvie Daviero-Minaud,[†] and Myung-Hwan Whangbo[‡]

Unité de Catalyse et de Chimie du Solide, CNRS UMR 8181, ENSC Lille - UST Lille, BP 90108, 59652 Villeneuve d'Ascq cedex, France, and Department of Chemistry, North Carolina State University, Raleigh, North Carolina 27695-8204

Received January 8, 2010; E-mail: houria.kabbour@univ-lille1.fr

Abstract: The two cobalt hexagonal perovskites 6H-$Ba_6Co_6F_{0.93}O_{16}$ and 10H-$Ba_5Co_5F_{0.77}O_{12.88}$ were prepared, and their structures were examined by X-ray and neutron diffraction and by ^{19}F solid state NMR spectroscopy. The magnetic and transport properties of these compounds were probed by magnetic susceptibility and electrical resistivity measurements, and their electronic structures by density functional and tight-binding calculations. The [$BaOF_{1-x}$] layers of these compounds create corner-sharing tetrahedral Co_2O_7 dimers at the interface between their face-sharing octahedral oligomers. Our density functional calculations leads to an unambiguous charge distribution model, which assigns high-spin Co^{3+} ions for the tetrahedral sites and low-spin Co^{3+}/Co^{4+} ions for the octahedral sites, and this model should be valid for the parent $BaCoO_{3-\delta}$ and the related oxychlorides and oxybromides as well. The F^- vacancies in the [$BaOF_{1-x}$] layers cause a strong distortion in the tetrahedral dimer Co_2O_7, which in turn affects the spin orientation of the high-spin Co^{3+} ions of the CoO_4 tetrahedra, i.e., parallel to the *c*-direction in $Ba_6Co_6F_{1-x}O_{16-\delta}$ but perpendicular to the *c*-direction in $Ba_5Co_5F_{1-x}O_{13-\delta}$. This difference in the spin orientations is related to the d-states of the distorted CoO_4 tetrahedra with high-spin Co^{3+} (d^6) ion on the basis of tight binding calculations and spin−orbit coupling as perturbation.

1. Introduction

The physical properties of transition metal oxides are strongly influenced by anion (i.e., O^{2-}) vacancies. Representative examples are the cuprates with high-temperature superconductivity and the manganates with giant magnetoresistance in which the oxygen stoichiometry governs their complex transport and magnetic properties, respectively. In solid oxide fuel cell electrodes, the ratio of electronic to ionic conductivity is tuned by oxygen vacancies.[1] The arrangement of anionic vacancies in an ordered or disordered manner opens extra possibilities in materials chemistry. Recently, a topotactic reduction of $SrFeO_{3-x}$ was found to produce the end-member $SrFeO_2$, which consists of FeO_2 layers made up of corner-sharing FeO_4 square planes with high-spin Fe^{2+} ions. This layered compound undergoes a three-dimensional magnetic ordering at a surprisingly high temperature ($T_N = 473$ K).[2] The electrochemical intercalation of oxygen in the Brownmillerite-type oxygen-deficient perovskites, $A_2M_2O_5$, is controlled by the vacancy ordering in the metastable phases $A_2B_2O_{5+\delta}$,[3] as found for $Sr_2Co_2O_5$,[4] $Sr_2Fe_2O_5$,[5] and $Ca_2Fe_2O_5$.[4b]

For a long time, the fluorine insertion in transition metal oxides such as Ruddlesden−Popper phases and Brownmillerites has been studied with the aim of modifying and tuning their physical properties.[6] For example, the fluorination of an antiferromagnet $Sr_2Mn_2O_5$ leads to $Sr_2Mn_2(O,F)_6$, which exhibits a ferromagnetic upturn,[7] while that of a non-superconducting oxide Sr_2CuO_3 gives rise to a superconductor $Sr_2CuO_2F_{2+\delta}$.[8] In most cases, the sites for the F^- ions can also accommodate O^{2-} ions. To distinguish the specific roles that the F^- and O^{2-} ions play, it is desirable to study compounds with different sites for

[†] Unité de Catalyse et de Chimie du Solide, CNRS UMR 8181.
[‡] North Carolina State University.

(1) (a) Brandon, N. P.; Skinner, S.; Steele, B. C. H. *Annu. Rev. Mater. Res.* **2003**, *33*, 183. (b) Matsuzaki, Y.; Yasuda, I. *Solid State Ionics* **1999**, *126*, 307. (c) Jorgensen, M. J.; Primdahl, S.; Bagger, C.; Mogensen, M. *Solid State Ionics* **2001**, *139*, 1. (d) Tarankón, A.; Skineer, S. J.; Chater, R. J.; Hernández-Ramírez, F.; Kilner, J. A. *J. Mater. Chem.* **2007**, *17*, 3175.

(2) (a) Tsujimoto, Y.; Tassell, C.; Hayashi, N.; Watanabe, T.; Kageyama, H.; Yoshimura, K.; Takano, M.; Ceretti, M.; Ritter, C.; Paulus, W. *Nature (London)* **2007**, *450*, 1062. (b) Hayward, M. A.; Rosseinsky, M. J. *Nature (London)* **2007**, *450*, 960. (c) Xiang, H. J.; Wei, S.-H.; Whangbo, M.-H. *Phys. Rev. Lett.* **2008**, *100*, 167207.

(3) (a) Abakumov, A. M.; Rozova, M. G.; Pavlyuk, B. P.; Lobanov, M. V.; Antipov, E. V.; Lebedev, O. I.; Van Tendeloo, G.; Sheptyakov, D. V.; Balagurov, A. M.; Bouree, F. *J. Solid State Chem.* **2001**, *158*, 100–111. (b) Abakumov, A. M.; Rozova, M. G.; Pavlyuk, B. P.; Lobanov, M. V.; Lebedev, O. I.; Van Tendeloo, G.; Ignatchik, O. L.; Ovtchenkov, E. A.; Koksharov, Yu., A.; Vasil'ev, A. N.; Antipov, E. V. *J. Solid State Chem.* **2001**, *160*, 353–361.

(4) (a) Le Toquin, R.; Paulus, W.; Cousson, A.; Prestipino, C.; Lamberti, C. *J. Am. Chem. Soc.* **2006**, *128*, 13161. (b) Paulus, W.; Schober, H.; Eibl, S.; Johnson, M.; Berthier, T.; Hernandez, O.; Ceretti, M.; Plazanet, M.; Conder, K.; Lamberti, C. *J. Am. Chem. Soc.* **2008**, *130*, 16080–16085.

(5) Takano, M.; Okita, T.; Nakayama, N.; Bando, Y.; Takeda, Y.; Yamamoto, O.; Goodenough, J. B. *J. Solid State Chem.* **1988**, *73*, 140–150.

(6) Mc Cabe, E. E.; Greaves, C. *J. Fluorine Chem.* **2007**, *128*, 448.

(7) Lobanov, M. V.; Abakumov, A. M.; Sidorova, A. V.; Rozova, M. G.; D'yachenko, O. G.; Antipov, E. V.; Hadermann, J.; van Tendeloo, G. *Solid State Sci.* **2002**, *4*, 19.

(8) Al-Mamouri, M.; Edwards, P. P.; Greaves, C.; Slaski, M. *Nature (London)* **1994**, *364*, 382.

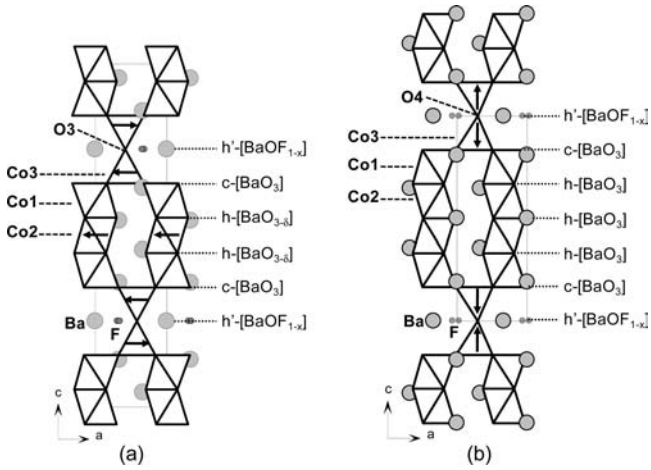

Figure 1. Crystal and magnetic structures of (a) $Ba_5Co_5F_{1-x}O_{13-\delta}$ and (b) $Ba_6Co_6F_{1-x}O_{16-\delta}$ as refined from the PND analyses. The cobalt centered polyhedrons are represented. For each structure, the layers types and their stacking sequence are indicated. Large light gray circles represent the barium atoms and the small dark gray circles represent the splitted fluorine atoms. Arrows on the cobalt centered polyhedrons indicate the magnetic moments directions of the magnetic atoms. The magnetic atoms are Co3 in both structures and Co2 (smaller magnetic moment) in (a).

the F^- and O^{2-} ions. Hexagonal perovskites containing F^- and O^{2-} ions provide such an opportunity.

In Ba-based hexagonal perovskites, the introduction of halide ions X^- (X = F, Cl) leads to halide-anion-deficient $[BaOX_{1-\delta}]$ layers, which favor a hexagonal-type (h-type) layer over a cubic-type (c-type) layer favored by the $[BaO_3]$ layers (Figure 1).[9] The h-type layer yields XBa_5 trigonal pyramids. As reported for 10H-$BaFeO_{2.8}$[10] and 10H-$BaMn_{0.4}Fe_{0.6}O_{2.73}$,[11] there are examples in which the "$[BaO_2]$" layers appear to be h-type layers. However, the oxygen atoms associated with the OBa_5 trigonal bipyramids have the bond valence sum (BVS) of approximately −0.5 instead of −2 expected for O^{2-}, and the structure optimization for the hypothetical 6H-$Ba_6Co_6O_{17}$ by density functional calculations leads to a severely distorted structure.[12] These observations suggest the possibility of "[BaO□]" layers rather than "$[BaO_2]$" layers in those structures.

In the present work we probe the question of how F^--anion vacancies in the h-type $[BaOF_{1-x}]$ layers of 6H-$Ba_6Co_6F_{1-x}O_{16-\delta}$ and 10H-$Ba_5Co_5F_{1-x}O_{13-\delta}$ affect their structural and physical properties. We examine this question on the basis of X-ray/neutron diffraction, transport/magnetic measurements, ^{19}F NMR spectroscopy, density functional and tight-binding calculations.

2. Experimental Section

Synthesis. Powder and Single crystals of 6H-$Ba_6Co_6F_{1-x}O_{16-\delta}$ and 10H-$Ba_5Co_5F_{1-x}O_{13-\delta}$ were obtained from a mixture of BaO_2, BaF_2 and Co_3O_4 as described in ref 12. In order to prepare a large amount of polycrystalline $Ba_5Co_5F_{1-x}O_{13-\delta}$ for neutron diffraction experiment, BaO_2 and Co_3O_4 were mixed in a stoichiometric ratio while BaF_2 was added in slight excess. This mixture was introduced in a gold tube sealed and heated up to 1030 °C (2.5 °C/min) for 72 h. The product was finally washed with warm water to remove the excess of BaF_2.

X-ray and Neutron Diffraction. Room temperature single crystal XRD was carried out on a Bruker SMART CCD-1K diffractometer using the Mo Kα radiation. The high temperature (230 and 550 °C) single crystal XRD analyses were performed using a heating NONIUS goniometric system. Intensities were extracted and corrected from the Lorentz-polarization factor through the SAINT program.[13] An empirical absorption correction was then applied using the SADABS program.[14] High-resolution neutron powder diffraction analysis was carried out at the LLB (Laboratoire Léon Brillouin). The 3T2 instrument ($\lambda = 1.2$ Å) was used in order to determine accurate room temperature crystal structures. The magnetic structures were refined from data collected with the G41 diffractometer ($\lambda = 2.426$ Å). Refinements were carried out using the Fullprof program.[15]

Magnetic Susceptibility and Electric Resistivity. The magnetic susceptibility was measured using an OXFORD Maglab Exa 9T magnetometer under a field of 1 T. Data were corrected from core electron diamagnetism. The transport measurements were carried out on the Maglab system equipped with a four-probe apparatus on dense barlike samples, pressed in an isostatic press (2000 bar). Gold wires were placed on the sintered pellets (500 °C) and fixed with colloidal silver paint. The resistivity was finally calculated by taking into account the shape and the size of the sample.

^{19}F Solid State NMR Spectroscopy. NMR measurements were performed at 376.3 MHz on an Advance 400 WB Bruker spectrometer (9.4 T) equipped with a 2.5 mm probe operating at 25−33 kHz MAS frequencies. Depending on the transverse coherence relaxation time, the ^{19}F MAS NMR spectra were acquired using the standard single-pulse acquisition or a $\pi/2-\tau-\pi-\tau$ spin−echo experiment. BaF_2 and $Ba_5Co_5F_{1-x}O_{13-\delta}$ analyses were performed with the single-pulse acquisition using a radio frequency field of 75 kHz, a relaxation delay of 2 s, and 32 and 1024 scans, respectively. $Ba_6Co_6F_{1-x}O_{16-\delta}$ was analyzed with the spin−echo sequence using radio frequency field of 75 kHz (pulse lengths of 3.3 and 6.6 μs for the $\pi/2$ and π pulses, respectively), a rotor synchronized echo delay of 250 μs, 256 scans, and a relaxation delay of 2 s. Different experiments were performed on each sample with variable spinning frequencies to unambiguously determine the isotropical shift. The ^{19}F chemical shifts were referred to the secondary reference CaF_2 (−108 ppm).

Density Functional Calculations. DFT calculations were performed using the Vienna *ab* initio simulation package (VASP).[16] The calculations were carried out within the generalized gradient approximation (GGA) for the electron exchange and correlation corrections using the Perdew−Wang[17] functional and the frozen core projected wave vector method.[18] The full geometry optimizations were carried out using a plane wave energy cutoff of 550 eV and 6*k* points in the irreducible Brillouin zone (convergence was checked up to 24*k* points). All structural optimizations converged with residual Hellman−Feynman forces on the atoms smaller than 0.03 eV/Å. For the calculations of density of states (DOS), the experimental structure was used. GGA plus on-site repulsion

(9) (a) Darriet, J.; Subramanian, M. A. *J. Mater. Chem.* **1995**, *5*, 543. (b) Quarez, E.; Abraham, F.; Mentré, O. *J. Solid State Chem.* **2003**, *176*, 137. (c) Bendraoua, A.; Quarez, E.; Abraham, F.; Mentré, O. *J. Solid State Chem.* **2004**, *177*, 1416.
(10) (a) Gomez, M. I.; Lucotti, G.; de Moran, J. A.; Aymonimo, J. M.; Pagola, S.; Stephens, P.; Carbonio, R. E. *J. Solid State Chem.* **2001**, *160*, 17. (b) Delattre, J. L.; Stacy, A. M.; Siegrist, T. *J. Solid State Chem.* **2004**, *177*, 928.
(11) Miranda, L.; Ramírez-Castellanos, J.; Hernando, M.; Varela, A.; González-Calbet, J. M.; Parras, M. *Eur. J. Inorg. Chem.*, **2007**, *15*, 2129.
(12) Ehora, G.; Renard, C.; Daviero-Minaud, S.; Mentré, O. *Chem. Mater.* **2007**, *19*, 2924.
(13) *SAINT: Area-Detector Integration Software*; Siemens Industrial Automation, Inc.: Madison, WI, 1995.
(14) *SADABS: Area-Detector Absorption Correction*; Siemens Industrial Automation, Inc.: Madison, WI, 1996.
(15) Rodriguez-Carvajal, J. *Physica B* **1993**, *192*, 55 (Fullprof program available from http://www-llb.cea.fr/fullweb/fp2k/fp2k.htm).
(16) Kresse G.; Furthmüller J. *Vienna Ab-initio Simulation Package (VASP)*; Institut für Materialphysik: Vienna, 2004; http://cms.mpi.univie.ac.at/vasp.
(17) Perdew, J. P.; Wang, Y. *Phys. Rev. B* **1992**, *45*, 13244.
(18) Kresse, G.; Joubert, D. *Phys. Rev. B* **1999**, *59*, 1758.

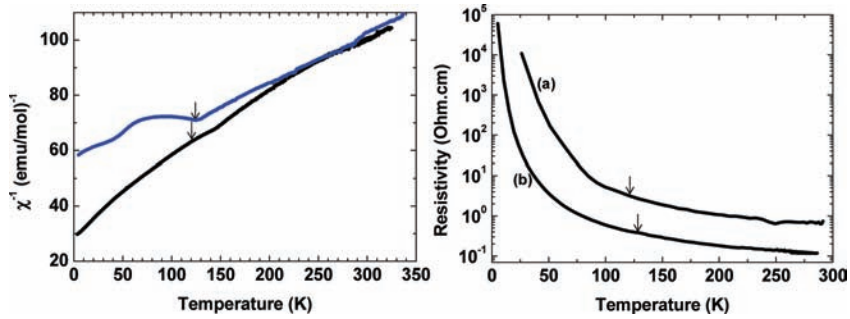

Figure 2. Inverse of the magnetic susceptibility (on the left) as a function of temperature for $Ba_5Co_5F_{1-x}O_{13-\delta}$ (black line) and $Ba_6Co_6F_{1-x}O_{16-\delta}$ (blue line). Resistivity as a function of temperature (on the right) for (a) $Ba_5Co_5F_{1-x}O_{13-\delta}$ and (b) $Ba_6Co_6F_{1-x}O_{16-\delta}$. In both cases, the arrows point toward T_N (122 and 126 K for $Ba_5Co_5F_{1-x}O_{13-\delta}$ and $Ba_6Co_6F_{1-x}O_{16-\delta}$, respectively).

(GGA+U)[19] calculations were also employed to account for the strong electron correlation associated with the 3d electrons on the Co atoms. A plane wave energy cutoff of 400 eV, a total energy convergence threshold of 10^{-6} and 30*k* points in the irreducible Brillouin zone were used. Both the geometry optimizations and DOS calculations were performed using an antiferromagnetic (AFM) spin configuration as found experimentally. For $Ba_5Co_5FO_{13}$, the orthorhombic subgroup *Cmcm* of the hexagonal space group $P6_3/mmc$ was used to describe fully occupied crystallographic positions. The hexagonal and the orthorhombic cell parameters are related as: $a_{ortho} = a_{hex}$, $b_{ortho} = b_{hex} \times \sqrt{3}$, $c_{ortho} = c_{hex}$.

3. General Structural and Magnetic Features of Halogen-Doped Hexagonal Perovskites

From the viewpoint of coordinate polyhedra, the crystal structure of 6H-$Ba_6Co_6F_{1-x}O_{16-\delta}$ (10H-$Ba_5Co_5F_{1-x}O_{13-\delta}$) consists of face-sharing octahedral tetramers (trimers) that are interconnected via corner-sharing to the corner-sharing tetrahedral dimers Co_2O_7 to form a 3D structure (Figure 1).[12] Each CoO_4 tetrahedron of the Co_2O_7 dimers caps three octahedral oligomers. If the octahedral oligomers are capped with isolated terminal CoO_4 tetrahedra, then the resulting structure is an isolated two-dimensional (2D) slab, as observed in the 5H and 12H $BaCoO_{3-\delta}$ polytypes.[20,21]

In discussing the oxygen vacancies and the doped F sites of 6H-$Ba_6Co_6F_{1-x}O_{16-\delta}$ and 10H-$Ba_5Co_5F_{1-x}O_{13-\delta}$, it is convenient to describe their structures from the viewpoint of stacking the $[BaOF_{1-x}]$ and $[BaO_3]$ layers. The stacking sequences corresponding to the 6H-$Ba_6Co_6F_{1-x}O_{16-\delta}$ and 10H-$Ba_5Co_5F_{1-x}O_{13-\delta}$ are (ch′chhh) and $(ch'chh)_2$, respectively (Figure 1), where c and h represent cubic- and hexagonal-type $[BaO_3]$ layers, respectively, and h′ represents a hexagonal-type $[BaOF_{1-x}]$ layer in which the O and F atoms occupy distinct crystallographic sites.[12] In these sequences, the cubic-$[BaO_3]$ layers break the face-sharing octahedral chains, while the stacking between this cubic-$[BaO_3]$ layer and the h′-$[BaOF_{1-x}]$ layer forms the tetrahedral entities. 6H-$Ba_6Co_6F_{1-x}O_{16-\delta}$ and 10H-$Ba_5Co_5F_{1-x}O_{13-\delta}$ are isomorphous with the corresponding oxochlorides that have been intensively investigated for their anisotropic transport and magnetic properties.[22,23] The replacement of hexagonal-$[BaOF_{1-x}]$ layers with cubic-$[BaO_2]$ layers leads to the 5H[20] trimeric and 12H[21] tetrameric polytypes of $BaCoO_{3-\delta}$. Their replacement with $[BaO_2Br]$ double layers yields a greatest disconnection between the terminal CoO_4.[24,25] In these oxides, there is no consensus about their charge distribution.

Typically, powder neutron diffraction (PND) experiments on these series of compounds showed rather large magnetic moments (1.94−3.42 μ_B) on the tetrahedral-site Co atoms, but small moments (0−1.05 μ_B) on the octahedral-site Co atoms. Provided that the octahedral oligomers plus the tetrahedra connected to them are considered as building blocks (differently connected, depending on the nature of the central layer, e.g. $[BaO_2]$, $[BaOX_{1-x}]$, $[BaO_2Br]$), the moments within each block order ferromagnetically.[24] The magnetic interactions between such blocks appear to depend on the structural connection between them through the CoO_4 tetrahedra.[20b,21,24,25]

4. Magnetic Properties of the Fluorine-Doped Hexagonal Perovskites

The analyses of the inverse magnetic susceptibilities vs *T* for the two compounds (Figure 2) lead to $\mu_{eff} = 6.82\ \mu_B$ per formula unit (FU) and $\theta_{CW} = -278$ K for $Ba_6Co_6F_{1-x}O_{16-\delta}$, and $\mu_{eff} = 7.16\ \mu_B$/FU and $\theta_{CW} = -345$ K for $Ba_5Co_5F_{1-x}O_{13-\delta}$, so that both compounds have dominant AFM interactions, which is similar to their oxychloride isomorphs.[23] For the latter, the Curie−Weiss law is not fully set at room temperature, and μ_{eff} and θ_{CW} have been roughly estimated from the data in the 250−330 K region. The θ_{CW} values show that the dominant AFM interactions are stronger in the $Ba_5Co_5F_{1-x}O_{13-\delta}$ than in $Ba_6Co_6F_{1-x}O_{16-\delta}$.

The broad anomalies marked by arrows in Figure 2 are due to the three-dimensional (3D) magnetic ordering. The Néel temperatures T_N are more accurately determined with the help of the PND study (Figure 3); $T_N = 126$ K for $Ba_6Co_6F_{0.93}O_{16}$, and $T_N = 122$ K for $Ba_5Co_5F_{0.77}O_{12.88}$. Below T_N, the magnetic reflections appear and can be indexed using the propagation vectors $k = (0, 0, 1/2)$ and $k = (0, 0, 0)$, respectively.

(19) Dudarev, S. L.; Botton, G. A.; Savrasov, S. Y.; Humphreys, C. J.; Sutton, A. P. *Phys. Rev. B* **1998**, *57*, 1505.
(20) (a) Parras, M.; Varela, A.; Seehofer, H.; Gonzalez-Calbet, J. M. *J. Solid State Chem.* **1995**, *120*, 327. (b) Boulahya, K.; Parras, M.; Gonzalez-Calbet, J. M.; Amador, U.; Martinez, J. L.; Tissen, V.; Fernandez-Diaz, M. T. *Phys. Rev. B* **2005**, *71*, 144402.
(21) Jacobson, A. J.; Hutchison, J. L. *J. Solid State Chem.* **1980**, *35*, 334.
(22) Kauffmann, M.; Mentré, O.; Legris, A.; Hébert, S.; Pautrat, A.; Roussel, P. *Chem. Mater.* **2008**, *20*, 1741.
(23) (a) **10H form**: Yamamura, K.; Young, D. P.; Siegrist, T.; Besnard, C.; Svensson, C.; Liu, Y.; Cava, R. J. *J. Solid State Chem.* **2001**, *158*, 175. (b) Tancret, N.; Roussel, P.; Abraham, F. *J. Solid State Chem.* **2005**, *178*, 3066. (c) Wang, H.; Yang, J.; Zhang, Z.; Dong, C.; Fang, M. *Phys. Lett. A* **2009**, *373*, 4092. (d) **6H form**: Kauffmann, M.; Mentre, O.; Legris, A.; Tancret, N.; Abraham, F.; Roussel, P. *Chem. Phys. Lett.* **2006**, *432*, 88.
(24) Mentré, O.; Kauffmann, M.; Ehora, G.; Daviero-Minaud, S.; Abraham, F.; Roussel, P. *Solid State Sci.* **2008**, *10*, 471.
(25) Kauffmann, M.; Roussel, P. *Acta Crystallogr., Sect. B* **2007**, *63*, 589.

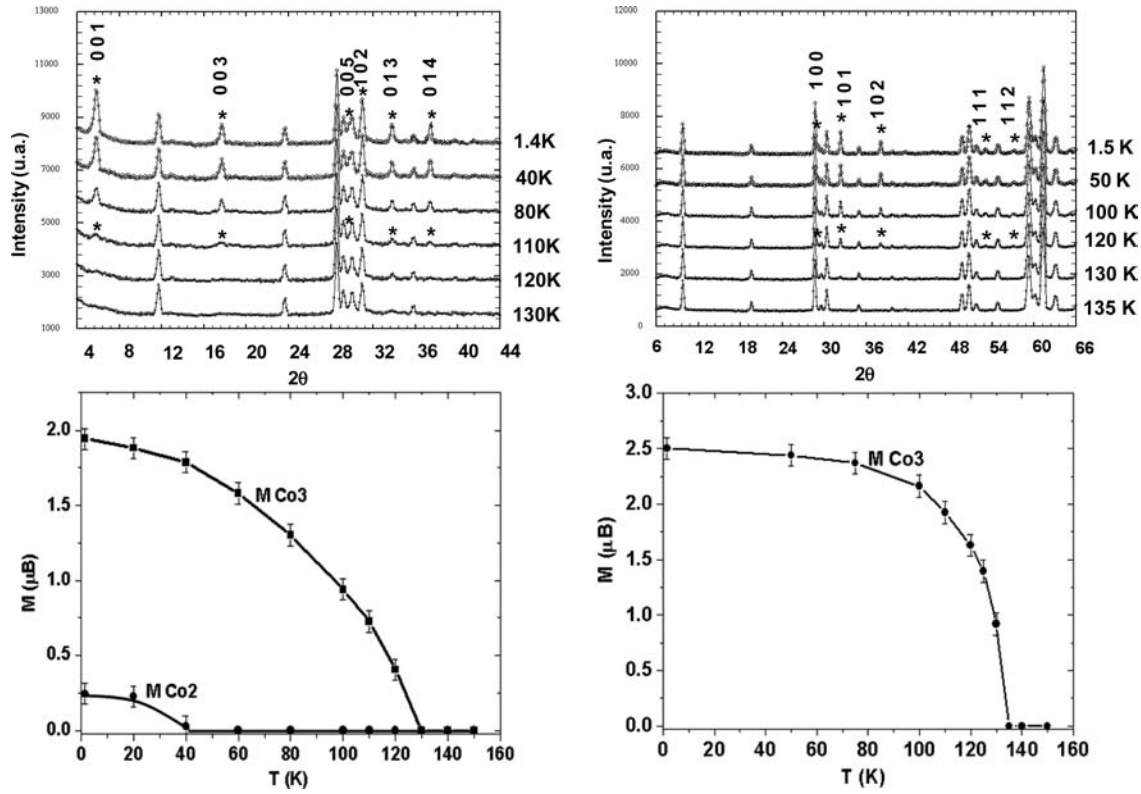

Figure 3. Evolution of the neutron powder diffraction pattern and of the local cobalt atoms magnetic moments (Co2 and/or Co3) as a function of temperature, in $Ba_5Co_5F_{1-x}O_{13-\delta}$ (on the left) and $Ba_6Co_6F_{1-x}O_{16-\delta}$ (on the right). Magnetic peaks on the powder diffraction patterns are indexed.

$Ba_6Co_6F_{1-x}O_{16-\delta}$ shows no 00*l* magnetic satellite so that the magnetic moments are parallel to the *c*-axis, while $Ba_5Co_5F_{1-x}O_{13-\delta}$ has no *hk*0 magnetic satellite so that the magnetic moments are perpendicular to the *c*-axis (Figure 3). On this basis, the magnetic structures were refined (Figure S9) with the following final reliability factors: For $Ba_6Co_6F_{1-x}O_{16-\delta}$ at $T = 1.5$ K: $R_{magn} = 10.70\%$, $\chi^2 = 2.40$, μ(Co3) = 2.54(4) μ_B, μ(Co1) = 0.0(9) μ_B, μ(Co2) = 0.05(8) μ_B. For $Ba_5Co_5F_{1-x}O_{13-\delta}$ at $T = 1.4$ K: $R_{magn} = 5.01\%$, $\chi^2 = 4.77$, μ(Co3) = 1.97(5) μ_B, μ(Co1) = 0.04(4) μ_B, μ(Co2) = 0.28(6) μ_B. Attempts to deviate the moments from these axes did not converge.

As in the case of the oxychlorides and oxybromides, the magnetic moments are either zero or weak on the octahedral-site Co atoms but significant on the tetrahedral-site Co atoms. The temperature dependence of these moments is shown in Figure 3. For $Ba_5Co_5F_{1-x}O_{13-\delta}$ the moments of the tetrahedral-site Co atoms lie in the *ab*-plane and a small moment appears below 60 K on the central octahedral-site Co2 atoms. The consideration of this latter in the Rietveld refinement process is essential for a good convergence. Otherwise, R_{magn} increases to ~10%. In fact, some of the magnetic satellites (003, 005, ...) show a weak but visible change in the intensity below 60 K. Below this temperature, a broad EPR signal was observed on this compound while no signal exists above. The tetrahedral-site Co3 of $Ba_5Co_5F_{1-x}O_{13-\delta}$ has a smaller moment than does that of $Ba_6Co_6F_{1-x}O_{16-\delta}$ (i.e., 1.9 vs 2.5 μ_B).

In understanding those different magnetic anisotropic properties, between 10H-$Ba_5Co_5F_{1-x}O_{13-\delta}$ and 6H-$Ba_6Co_6F_{1-x}O_{16-\delta}$, it is crucial to understand how the F doping affects the oxygen vacancies and how the local structural distortions and the local electronic structures are influenced by the fluorine content and the oxygen vacancies. For the convenience of our discussion, the octahedral- and tetrahedral-site Co atoms will be hereafter referred to as the Co(O_h) and Co(T_d) atoms, respectively.

5. Anion Vacancies

The crystal structures of $Ba_6Co_6F_{1-x}O_{16-\delta}$ and $Ba_5Co_5F_{1-x}O_{13-\delta}$ were re-analyzed on the basis of their high resolution PND data as described in the Experimental Section and the previous paragraph. By comparing with the structures already reported,[12] we note the following:

(a) ^{19}F solid state NMR spectra show a single isotropic resonance for each compound centered at −192 and −14.1 ppm, for $Ba_6Co_6F_{1-x}O_{16-\delta}$ and $Ba_5Co_5F_{1-x}O_{13-\delta}$, respectively (Figure 4a,b). They are accompanied by a large number of spinning sidebands arising from the paramagnetic effects. At this stage, one should unambiguously deduce a single crystallographic site for F^-, likely in the h′-[$BaOF_{1-x}$] layers, while any partial substitution of the [BaO_3] layers is excluded. By comparison, the diamagnetic BaF_2 (Figure 4c) presents a signal at −14.4 ppm with a full width at half-maximum (fwhm) of 1200 Hz. The signals are much broader for the cobaltites (fwhm of 12600 Hz for $Ba_6Co_6F_{1-x}O_{16}$ and 4200 Hz for $Ba_5Co_5F_{1-x}O_{13}$) (see section 6).

(b) From the PND refinements, the site occupancies show that $x = 0.07(2)$ and $\delta = 0.0$ for $Ba_6Co_6F_{1-x}O_{16-\delta}$, while $x = 0.23(2)$ and $\delta = 0.12(1)$ for $Ba_5Co_5F_{1-x}O_{13-\delta}$. Thus, the average Co oxidation state is +3.49 for $Ba_6Co_6F_{1-x}O_{16-\delta}$, and +3.31 for $Ba_5Co_5F_{1-x}O_{13-\delta}$.

(c) In $Ba_6Co_6F_{1-x}O_{16-\delta}$, the O_3 faces of the octahedral tetramers are fully occupied. In $Ba_5Co_5F_{1-x}O_{13-\delta}$, however, the O_3 faces of the central two [BaO_3] layers in the octahedral trimers are 96% occupied. Consistent with this observation, $BaMnO_{3-\delta}$ polytypes show a strong tendency for the oxygen

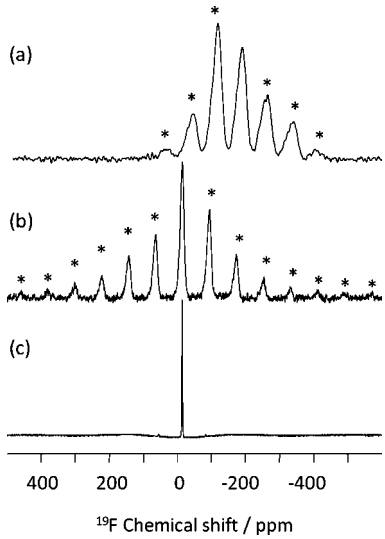

Figure 4. ^{19}F MAS NMR spectra of $Ba_6Co_6F_{1-x}O_{16-\delta}$ (a), $Ba_5Co_5F_{1-x}O_{13-\delta}$ (b), and BaF_2 (c). (a) was obtained with a spin−echo sequence, and (b) and (c) spectra were acquired with the standard single-pulse acquisition. * show the spinning sidebands.

vacancies to be in the h-type layers rather than in the c-type layers. This tendency is explained by the influence of the barium atoms, more electropositive than the transition metal atoms, through the Ba−O bonds which are shorter in the cubic layers. The resulting stronger bonding interaction, compared with the hexagonal layers, is less favorable for oxide removal.[26]

(d) In the central $[BaOF_{1-x}]$ layer of $Ba_6Co_6F_{1-x}O_{16-\delta}$, the apex oxygen atom of the CoO_4 tetrahedron (i.e., the shared-corner of the Co_2O_7 tetrahedral dimer) is displaced by $\Delta = 0.37$ Å from its central symmetric position, which is comparable to the displacement found for oxychloride compounds.[22] The corresponding displacement in $Ba_5Co_5F_{1-x}O_{13-\delta}$ is much stronger (i.e., $\Delta = 0.87$ Å). The Fourier maps calculated for the $[BaOF_{1-x}]$ layer show this effect clearly (Figure 5).

(e) The Fourier maps of Figure 5 show an anisotropic shape of the F atom. This results from the in-plane off-centering and the high thermal vibration due to the large cavity of the Ba_5 unit surrounding the F atom. For both $Ba_6Co_6F_{1-x}O_{16-\delta}$ and $Ba_5Co_5F_{1-x}O_{13-\delta}$, the splitting of the fluoride position improves the refinement factor, leading to a shift of ∼0.3 Å away from its central special position. For $Ba_5Co_5F_{1-x}O_{13-\delta}$, this splitting increases the mean F···O distances. For example, F(split)···O(split) distances are included in the [2.08−4.02 Å] range with 2/3 of them plausible because greater than the sum of the van der Waals radii (i.e., greater than 2.71 Å).

(f) $Ba_6Co_6F_{1-x}O_{16-\delta}$ and $Ba_5Co_5F_{1-x}O_{13-\delta}$ differ substantially in the occupancy of the off-centered F position, i.e., 93% for $Ba_6Co_6F_{1-x}O_{16-\delta}$ vs 77% for $Ba_5Co_5F_{1-x}O_{13-\delta}$.

(g) The final chemical formula and the R factors are: $Ba_6Co_6F_{0.93}O_{16}$, $\chi^2 = 1.35$, $R_F = 5.38\%$ and $R_{Bragg} = 5.90\%$, and $Ba_5Co_5F_{0.77}O_{12.88}$, $\chi^2 = 2.56$, $R_F = 5.86\%$ and $R_{Bragg} = 7.07\%$. Our previous single crystal data lead to similar results concerning the anion positions once their positions and occupancies are relaxed.[12]

In PND refinements, the difference between the O and F Fermi lengths is relatively small so that a mixed O/F occupancy might result for O and F positions. In two 10H-$BaFeO_{3-x}$ polytypes ($x = 0.2$, 0.35)[10] and 10H-$BaMn_{0.4}Fe_{0.6}O_{2.73}$,[11] the oxygen atoms were allowed to occupy the halogen-sites. In such a case, the trigonal bipyramidal OBa_5 associated with this site leads to a highly unreasonable BVS of the oxygen (i.e., ∼−0.5 instead of ∼−2). To remove this difficulty, one might imagine either the presence of a monovalent anion such as OH^- or that of anionic deficient [BaO□] layers (see Discussion in ref 12). For similar reasons, we propose $[Ba_1O_1F_{1-x}\square_x]$ layers in $Ba_6Co_6F_{1-x}O_{16-\delta}$ and $Ba_5Co_5F_{1-x}O_{13-\delta}$.

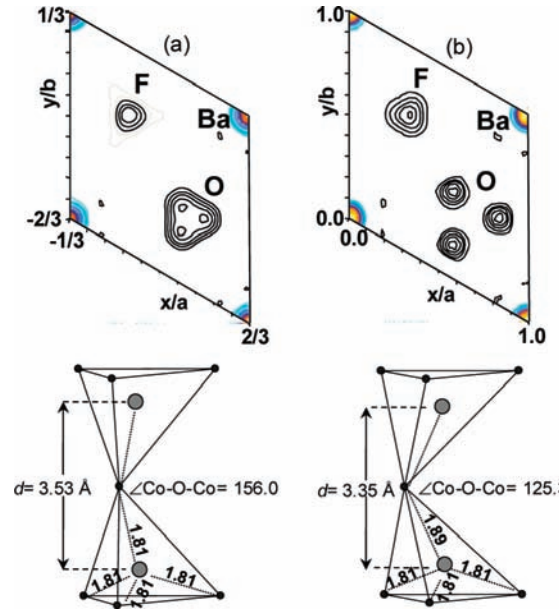

Figure 5. Fourier maps for the $[BaOF_{1-x}]$ layer of (a) $Ba_6Co_6F_{1-x}O_{16-\delta}$ and (b) $Ba_5Co_5F_{1-x}O_{13-\delta}$. The tetrahedral dimer Co_2O_7 corresponding to the Fourier map is shown underneath each map. Distances are given in (Å) and angles in (deg).

6. Spin Exchange of the Tetrahedral Dimer Co_2O_7

In the refined magnetic structures, the spins of the CoO_4 tetrahedra in each Co_2O_7 dimer are antiferromagnetically coupled, and the spin of each CoO_4 tetrahedron is ferromagnetically coupled to the spins of its adjacent octahedral oligomer. This observation was intensively discussed for $Ba_6Co_6Cl_{1-x}O_{16-\delta}$.[22] The strong distortions in the Co_2O_7 dimers of $Ba_5Co_5F_{1-x}O_{13-\delta}$ (Co···Co = 3.3 Å, ∠Co−O−Co = 125°) and $Ba_6Co_6F_{1-x}O_{16-\delta}$ (Co···Co = 3.5 Å, ∠Co−O−Co = 155°) are favorable for strong AFM spin exchange within the Co_2O_7 dimers. For both compounds, the AFM exchange J between the two Co^{3+} ions in each Co_2O_7 dimer is expected to be largely responsible for θ_{CW}. According to the mean field approximation, $\theta_{CW} = [zS(S+1)/3]J/k_B$, where z is the number of the magnetic ions interacting with a given Co3 with exchange J (namely, $z = 1$ in the present case), k_B is the Boltzmann constant, and $S = 2$ for the tetrahedral high-spin Co^{3+} ions (see section 8.3). Thus, it is estimated that $J/k_B = -139$ K for $Ba_6Co_6Cl_{1-x}O_{16-\delta}$ and −172 K for $Ba_5Co_5F_{1-x}O_{13-\delta}$. The latter is probably underestimated due to the poor linearity of the $\chi^{-1}(T)$ vs T plot in the investigated temperature range. In any event, the dimer exchange J values are significant. Then it is reasonable to assume that below T_N the interordering of the strongly antiparallel dimers occurs through the ferromagnetic oligomeric connections. The close Néel temperatures observed in those two compounds (122 and 126 K) pictures similar magnetic exchanges through trimers

(26) (a) Adkin, J. J.; Hayward, M. A. *Chem. Mater.* **2007**, *19*, 755. (b) Parras, M.; Alonso, J. M.; Gonzalez-Calbet, J. M.; Vallet-Regi, M. *J. Solid State Chem.* **1995**, *117*, 21.

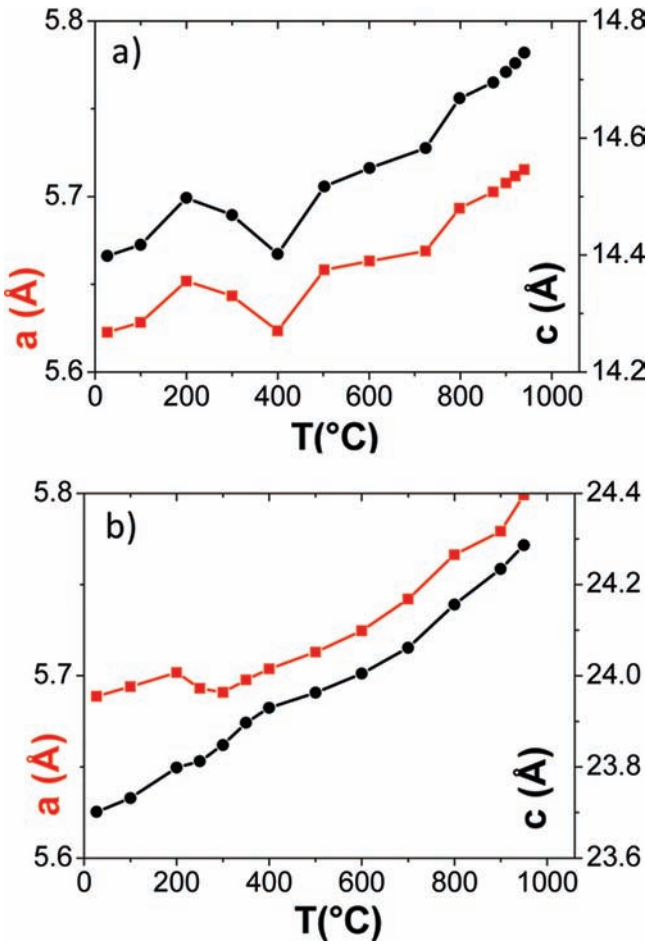

Figure 6. Evolution of the unit cell parameters *a* and *c* determined by high temperature XRD in (a) for $Ba_6Co_6F_{1-x}O_{16-\delta}$, and in (b) for $Ba_5Co_5F_{1-x}O_{13-\delta}$.

and tetramers. The different intra-Co_2O_7 exchanges might be at the origin of the difference between the ^{19}F solid state NMR spectra collected at room temperature under an applied field of 9.4 T. Further investigation would be necessary to better understand the latter observation.

7. High-Temperature XRD and Distortion of the Tetrahedral Dimer Co_2O_7

The lattice parameters of $Ba_6Co_6F_{1-x}O_{16-\delta}$ and $Ba_5Co_5F_{1-x}O_{13-\delta}$ refined from high-temperature XRD are presented in Figure 6, a and b respectively. For both $Ba_6Co_6F_{1-x}O_{16-\delta}$ and $Ba_5Co_5F_{1-x}O_{13-\delta}$, the lattice parameters *a* and *c* increase gradually with increasing temperature, except for contraction phenomena found around 200−400 °C. In $Ba_6Co_6F_{1-x}O_{16-\delta}$, both *a* and *c* are involved in this cell contraction (Figure 6a). This is related most likely to the creation of oxygen vacancies in the h-type [BaO_3] layers forming the octahedral tetramers. Indeed, let us consider an h-type [BaO_3] layer face shared by two octahedrons and the two apical Co atoms along *c*. The creation of a vacancy would affect both the *ab* plane and the *c* parameter through the concomitant impact on the intralayer *d*(Ba−O) bonds and of the modified Co−Co interaction.

In $Ba_5Co_5F_{1-x}O_{13-\delta}$, the cell contraction from 200 to 400 °C affects only the *ab*-plane (Figure 6b), which is caused most likely by the significant concentration of fluoride vacancies in the [$BaOF_{0.77}$] layer and the resulting distorted CoO_4 tetrahedron described above. The effect of the temperature would favor the symmetry gain through shifting the off-centered apex oxygen toward its central position.

The above suggestions concerning the anisotropic cell contraction on heating are confirmed by the high-temperature single-crystal XRD structures determined for $Ba_5Co_5F_{1-x}O_{13-\delta}$. The diffraction data were collected at room temperature, 230, and 550 °C on the same single-crystal sample. Since the crystal is fixed in a closed quartz capillary, exchanges with the surrounding atmosphere are strongly inhibited. Then, the occupancies of the oxygen anions were fixed while the occupancy of F^- was constrained to be equal for the three investigated temperatures, leading to similar F^- stoichiometry as deduced from the PND analysis. Table 1 summarizes the lattice parameters and some interatomic distances within the face-sharing octahedral trimer, the [$BaOF_{1-x}$] layer, and the corner-sharing tetrahedral dimer.

In the face-sharing octahedral trimers, all distances exhibit a weak temperature dependence. In sharp contrast, a significant temperature effect is found for the Co_2O_7 tetrahedral dimers, which strongly contributes to the increase in the *c*-parameter. The most striking effect is that the amplitude of the oxygen-atom split in the [$BaOF_{1-x}$] layer from its central position is reduced, while the cobalt atoms are displaced away from each other. These changes reduce the Co···O_{split} distance (1.85 Å from room temperature to 1.81 Å at 550 °C) and increase the ∠Co−O−Co angle and Co−Co distance (from 127° and 3.31 Å, respectively, at room temperature to 138° and 3.38 Å, respectively, at 550 °C).

The split of the shared corner of the Co_2O_7 dimers out of its three-fold axis positions is related to the high concentration of F^- vacancies in the [$BaOF_{1-x}$] layer, which favors the off-centering of the oxygen due to the associated electrostatic forces. As depicted in Figure 7, the large *in-plane* splitting of the oxygen positions ideally implies the presence of one F^- vacancy out of every three F^- ions (i.e., the occupancy of 67%), which is necessary for the O···F separations greater than 2.7 Å. However, experimentally, the F occupancy of 77% is found. This reflects most probably additional disorder in the oxygen positions, locally leading to a more central oxygen position, depicted by its large thermal parameter ($B = 2.71$ Å^2 from the room temperature ND refinement). The latter would create space for more F-filled nanodomains.

In order to computationally verify the influence of F vacancies on the local geometry, full structure relaxations (DFT calculations using the VASP) were carried out on orthorhombic unit cells in which the fluorine (in its ideal central position) site was either filled or emptied. Figure 8 shows the comparison between the experimental and the two optimized models. As detailed above, the experimental local geometry of the [$BaOF_{1-x}$] layer (Figure 8a) exhibits a short O3−F distance compatible only with an appropriate F/□ distribution (Figure 7). During the relaxation of the filled F structure (Figure 8b), there occurs a strong displacement of O3 toward its ideal central oxygen position. This rearrangement leads to ∠Co3−O3−Co3 = 160.6°, which is greater than found experimentally. In contrast, the optimized empty-F structure (Figure 8c) shows slight rearrangements; O3 remains roughly in its initial shifted position, and the O3−Ba distances are almost unchanged (i.e., 2.97−4.19 Å vs 2.95−4.15 Å experimentally). Similarly, the geometry of the relaxed Co_2O_7 dimer remains close to that of the experimental one. It is clear

Table 1. Characteristics of the Structures of $Ba_5Co_5F_{1-x}O_{13-\delta}$ Determined from Single-Crystal XRD at 30, 230, and 550 °C and from PND at 30 °C, Where the Distances Are Given in Å

(a) X-ray Data Collection and Structure Refinement Parameters for Single Crystal Data

crystal data	30 °C	230 °C	550 °C
formula	$Ba_5Co_5F_{1-x}O_{13-\delta}$	$Ba_5Co_5F_{1-x}O_{13-\delta}$	$Ba_5Co_5F_{1-x}O_{13-\delta}$
symmetry	hexagonal	hexagonal	hexagonal
Z	4	4	4
unit cell parameters (Å)	$a = 5.6878(11)$ $c = 23.701(5)$	$a = 5.6995(14)$ $c = 23.799(6)$	$a = 5.710(2)$ $c = 23.925(10)$
space group	$P6_3/mmc$	$P6_3/mmc$	$P6_3/mmc$
volume (Å^3)	664.013	669.525	675.611
λ (Mo Kα) (Å)	0.71073	0.71073	0.71073
θ range (deg)	3.44−28.45	3.42−28.72	3.41−28.60
scan mode	ω	ω	ω
h, k, l ranges	$-7 < h < 7$ $-7 < k < 7$ $-31 < l < 30$	$-7 < h < 5$ $-7 < k < 7$ $-26 < l < 31$	$-7 < h < 5$ $-7 < k < 6$ $-24 < l < 30$
measured reflections	4645	4776	4718
independent reflections	368	374	379
independent reflections ($I > 3\sigma(I)$)	295	319	312
absorption correction	analytical	analytical	analytical
absorption coefficient (mm^{-1})	10.341	10.256	20.375
R_{int}	0.0458	0.0377	0.0358
refinement method	least-squares on F^2	least-squares on F^2	least-squares on F^2
$F(000)$	1051	1051	1051
refined parameters/constraints	39/0	38/0	38/0
R(obs), R(all)	0.0223/0.0391	0.0227/0.0320	0.022/0.0328
R_w(obs), R_w(all)	0.0191/0.0208	0.0225/0.0234	0.0221/0.0230
extinction coefficient	0.0324(21)	0.0736(38)	0.0489(29)
max/min $\Delta\rho$ (e·A^3)	2.34/−1.93	1.40/−1.22	1.71/−1.25

(b) $[BaOF_{1-x}]$ layer; O_{split} Refers to the Corner Oxygen Shared between the Two CoO_4 Tetrahedra, and O_{cent} (2/3 1/3 1/4) to the Symmetrical Position of the Corner-Shared Oxygen before Splitting; F_{split} Refers to the Split F Atom

	30 °C	230 °C	550 °C	30 °C (neutron)
O3···O_{cent}	0.819(25)	0.791(10)	0.654(10)	0.8671(2)
F_{split}···O_{split}	2.20(17)−3.94(16)	2.16(5)−3.98(5)	2.28(5)−3.91(5)	2.081(1)−4.025(1)

(c) Corner-Sharing Tetrahedral Dimer $[Co_2O_7]$; Co_{Td} Refers to the Co Atom at the Tetrahedral Site, O_{basal} to the Oxygen Atoms on the Basal Plane of the CoO_4 Tetrahedron

	30 °C	230 °C	550 °C	30 °C (neutron)
Co_{Td}···O_{split}	1.849(12)	1.850(4)	1.815(4)	1.888(1)
Co_{Td}···O_{basal}	1.828(5) × 3	1.828(2) × 3	1.826(3) × 3	1.816(1) × 3
Co_{Td}···Co_{Td}	3.315(2)	3.344(2)	3.385(2)	3.355(1)
intertrimer	4.690(6)	4.726(7)	4.756(7)	4.639(1)

(d) Face-Sharing Octahedral Trimer Unit $[Co_3O_{12}]$; Co_{center} and Co_{edge} Refer Respectively to the Central and to the Edge Co Atoms of the Face-Sharing Octahedral Trimer

	30 °C	230 °C	550 °C	30 °C (neutron)
Co_{edge}···O	1.925(5) × 3	1.929(5) × 3	1.936(5) × 3	1.923(1) × 3
	1.952(3) × 3	1.959(3) × 3	1.972(3) × 3	1.971(1) × 3
Co_{center}···O	1.891(3) × 6	1.895(3) × 6	1.891(3) × 6	1.905(1) × 6
Co_{center}···Co_{edge}	2.495(1)	2.506(2)	2.519(2)	2.525(1)

from these model calculations that the F^- vacancies are responsible for the observed tetrahedral distortion.

8. Density Functional Analysis of the Oxidation States and Electron Configurations of the Co Atoms

In discussing the magnetic properties of $Ba_5Co_5F_{1-x}O_{13-\delta}$ and $Ba_6Co_6F_{1-x}O_{16-\delta}$, it is necessary to probe the oxidation states and the electron configurations appropriate for their octahedral and tetrahedral Co atoms. For this purpose, we performed density functional calculations for the hypothetical structure $Ba_5Co_5FO_{13}$ (i.e., $Ba_5Co_5F_{1-x}O_{13-\delta}$ with $x = \delta = 0$) with the ordered spin arrangement as found experimentally for $Ba_5Co_5F_{1-x}O_{13-\delta}$. The subgroup *Cmcm* of the experimental crystal space group (i.e., $P6_3/mmc$) was used to describe the one-third occupied O3 site into a filled site. Since the F splitting is small, the F atom was kept at its symmetrical position.

8.1. Density of States Analysis for $Ba_5Co_5FO_{13}$ in the GGA Approximation. Our GGA calculations predict $Ba_5Co_5FO_{13}$ to be metallic. Although this result is not consistent with the fact that $Ba_5Co_5F_{1-x}O_{13-\delta}$ is a magnetic insulator, the general features of the electronic structure of $Ba_5Co_5FO_{13}$ obtained from the GGA calculations are relevant for our discussion of the probable oxidation states and spin configurations of the octahedral and tetrahedral site Co atoms (see below for further discussion). The plots of the total and projected DOS calculated for the Co1, Co2, and Co3 atoms, presented in Figure 9, show that the Co1 and Co2 atoms of the octahedra are in low-spin states. For Co1, the up- and the down-spin t_{2g} states

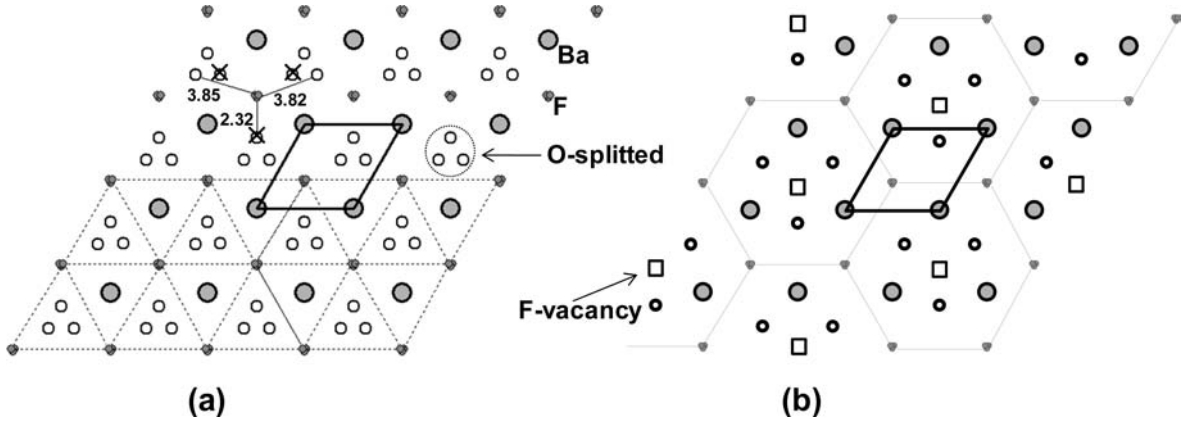

Figure 7. Projection view of the $[BaOF_{1-x}]$ layer of $Ba_5Co_5F_{1-x}O_{13}$ (a) with all possible positions for F^- and O^{2-} and (b) with F^- vacancies (empty squares) plus oxygen atoms selected to provide chemically meaningful F···O distances. The cross eliminates forbidden oxygen atoms around the central F.

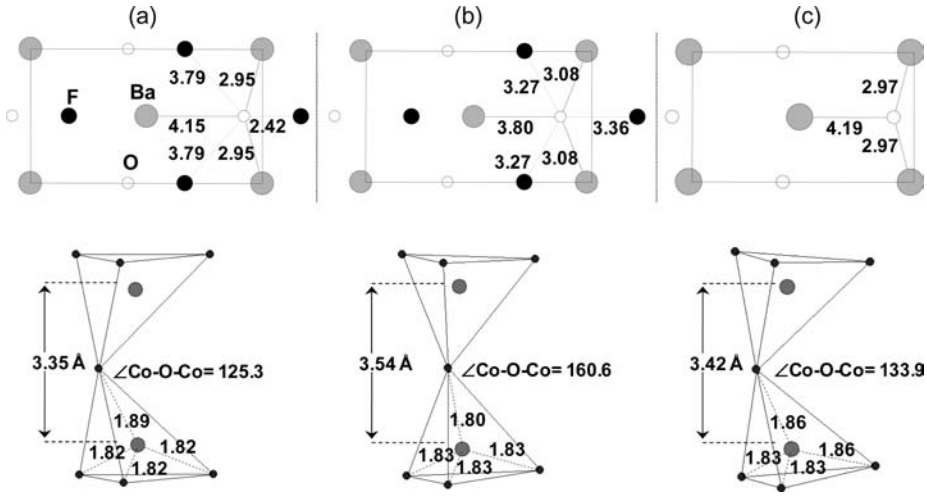

Figure 8. Local geometries (projection of $[BaOF_{1-x}]$ layer on top and tetrahedral dimers on bottom) in (a) the experimental structure of $Ba_5Co_5F_{0.77}O_{12.88}$, (b) the relaxed structure of $Ba_5Co_5FO_{13}$ and (c) the fluorine-less relaxed structure $Ba_5Co_5O_{13}$. All structures are represented in the orthorhombic unit cell. Distances are given in (Å) and angles in (deg).

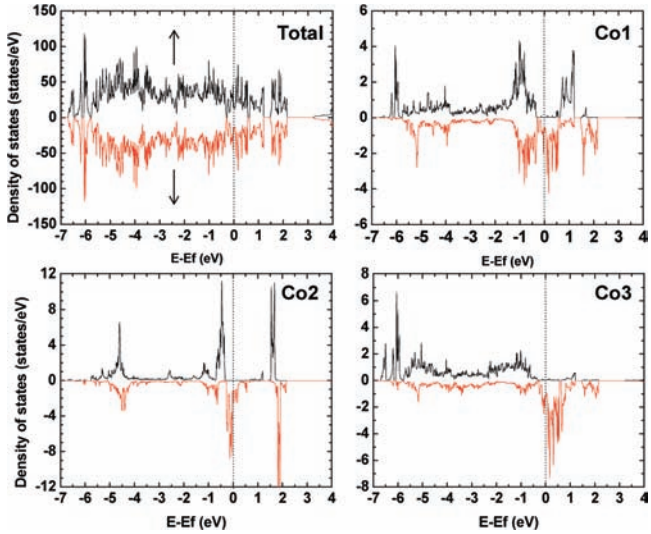

Figure 9. Total and projected DOS plots obtained for $Ba_5Co_5FO_{13}$ from GGA calculations.

lie in the ranges of −6.3 to −0.3 eV and −5.8 to 0.58 eV, respectively, while the up- and down-spin e_g states lie in the ranges of 0.5−1.7 eV and 0.6 to 2.2 eV, respectively. For Co2, the up- and the down-spin t_{2g} states lie in the ranges of −5.7 to −0.3 eV and −5.7 to 0.56 eV, respectively, while the up- and down-spin e_g states lie in the ranges of 1.1−1.7 eV and 1.6−2.2 eV, respectively. For both Co1 and Co2, the e_g states are empty, the up-spin t_{2g} states are fully occupied, while the down-spin t_{2g} states are partially empty, essentially leading to a low-spin d^5 configuration. The projected DOS plots for the tetrahedral Co3 atom suggest a high-spin state; the up-spin levels are all occupied with some occupied down-spin states such that the Co3 atom is best described by a high-spin d^6 configuration. The low-spin states predicted for the octahedral Co atoms Co1 and Co2 are consistent with the experimental data. The high-spin state predicted for the tetrahedral Co atom is reasonable, since the split between the *e* and t_2 states in a tetrahedral crystal field should be smaller than that between the t_{2g} and e_g states in an octahedral crystal field. The spin moments calculated for the Co1, Co2, and Co3 atoms, 0.82, 0.45, and 2.43 μ_B, respectively, are consistent with the above picture. The spin moment 2.43 μ_B for Co3 site seems too small compared with 4 μ_B expected for a high-spin Co^{3+} ion, but it should be noted that the three basal O atoms surrounding each Co3 atom carry the moment of 0.25 μ_B, so that the Co_3O_4 tetrahedral unit carries the spin moment of about 3.2 μ_B.

8.2. Model for Charge Distribution. The experimental spin moment value of Co(T_d) (1.9 μ_B), lower than expected for a high-spin Co^{3+} ion, led to the proposal of the intermediate spin

(IS) configuration for Co^{4+}.[22,24] However, this IS configuration is not supported by the present electronic structure calculations. Here, the value of the spin-only moment calculated for Co(T_d) should not be taken too literally, because the orbital moment arising from spin−orbit coupling (SOC) can increase the overall moment of Co(T_d) and because the moments of the oxygen atoms surrounding Co(T_d) (see above), which reflect the presence of covalent bonding in the Co−O bonds of the Co(3)O_4 tetrahedron, should not be neglected. On the basis of the calculated electronic structure, the charge distribution for $Ba_5Co_5F_{0.77}O_{12.88}$ and $Ba_6Co_6F_{0.93}O_{16}$ can be described by considering the high-spin Co^{3+} state for Co(T_d). Then, the Co(O_h) atoms of $Ba_5Co_5F_{0.77}O_{12.88}$ and $Ba_6Co_6F_{0.93}O_{16}$ are in the low-spin state with the average oxidation states +3.51 and +3.73, respectively. The high-spin Co^{3+}(T_d)/low-spin $Co^{3+/4+}$(O_h) description should be applicable to other oxyhalides that have similar structures.

As a consequence of the above discussion, the 5H- and 12H-$BaCoO_{3-\delta}$ polytypes deserve special attention since there is no clear consensus about their charge distribution. Both compounds display similar elementary blocks made up of the linear octahedral oligomers (i.e., trimers and tetramers in the 5H and in 12H phases, respectively) capped by terminal tetrahedral leading to the 2D structures. They are both characterized by a ferromagnetic ordering with local moments of ∼3.5−4.2 μ_B on the Co(T_d) and lower moments on the Co(O_h) atoms.[20b,21] Due to the rarity of Co^{4+} ions at tetrahedral sites in the literature, it has been assumed that the Co(T_d) site prefers a Co^{3+} ion.[20,21] Due to the similarity of the building blocks in structure and magnetic property (i.e., intrablock ferromagnetism), it is reasonable to suggest the high-spin Co^{3+}(T_d)/low-spin $Co^{3+/4+}$(O_h) description for the 5H- and 12H- $BaCoO_{3-\delta}$ polytypes. In addition, it should be noted that, starting from 1D-$BaCoO_3$ containing Co^{4+} ions, the CoO_4 tetrahedra at both sides of the oxygen-deficient [BaO_2] layers occurs upon reducing. This reinforces the suggestion that Co^{3+} ions are present at the Co(T_d) sites of these pseudo-1D series. The terminal disconnected CoO_4 tetrahedra favors the lowering of covalency effects, increasing the local Co(T_d) moments, as observed in the oxides and oxobromides.[24] Finally, the interblock couplings depend on the connection between terminal tetrahedra: AFM in the connected oxofluorides and oxochlorides, FM in the disconnected oxides, metamagnetism in the strongly disconnected oxobromides.[22−25,27]

8.3. Transport Properties. Both $Ba_6Co_6F_{1-x}O_{16-\delta}$ and $Ba_5Co_5F_{1-x}O_{13-\delta}$ are insulating antiferromagnets. In that sense, they are similar to $Ba_6Co_6Cl_{1-x}O_{16-\delta}$.[22] Recent experiments on single crystals of $Ba_5Co_5Cl_{1-x}O_{13-\delta}$ have evidenced a strong anisotropic electrical behavior with 2 orders of magnitude between ρ_{ab} (∼10^{-1} Ω·cm at room temperature) and ρ_c (∼10^{-3} Ω·cm at room temperature). Similar tendencies can be suggested for the two oxyfluorides examined in the present study. In the absence of large single crystals, transport properties have been investigated on sintered powder samples. Of the two compounds, $Ba_6Co_6F_{1-x}O_{16-\delta}$ has a lower resistivity. This can be assigned to a different charge distribution and subsequent concentration of carriers inside the octahedral trimers and tetramers as established in the section 8.2. Above T_N, the conductivity of the bulk obeys an Arrhenius law, with a rather low thermal dependence, E_a = 0.02 and 0.03 eV for $Ba_6Co_6F_{1-x}O_{16-\delta}$ and $Ba_5Co_5F_{1-x}O_{13-\delta}$, respectively. Transport anomalies have been found at T_N for the two chloride analogues,

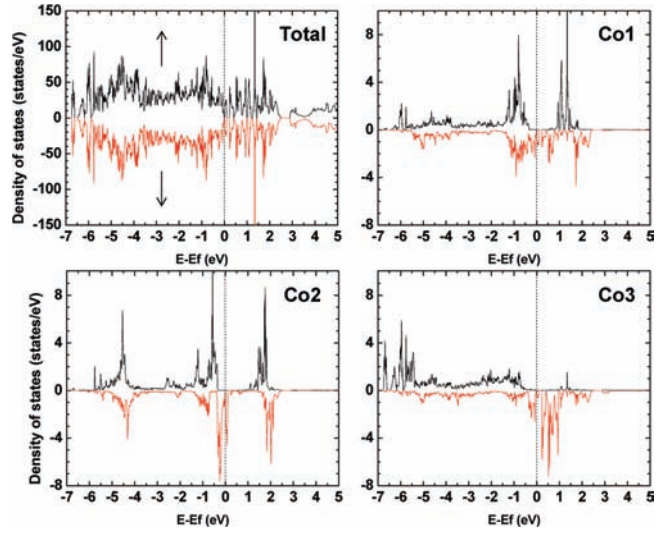

Figure 10. Total and projected DOS plots obtained for $Ba_5Co_5FO_{13}$ from GGA+U calculations (with U = 1 eV on the Co atoms).

and variable range hopping has been suggested but is complicated by their anisotropic transport. The two compounds clearly turn out to be strong insulators at low temperature.

Our GGA calculations predict $Ba_5Co_5FO_{13}$ to be metallic (Figure 9) while it is a magnetic insulator. Assuming that this incorrect prediction is due to the neglect of electron correlation of the Co 3d states, we carried out GGA+U calculations for $Ba_5Co_5FO_{13}$ with onsite repulsion U added on Co (U = 0−8 eV). These GGA+U calculations fail to provide a magnetic insulating state. However, only when the fluorine site was emptied (i.e., for $Ba_5Co_5O_{13}$ for which x = 1, δ = 0), the gap opening was achieved with U values as small as 1 eV. The DOS plots of $Ba_5Co_5O_{13}$ are shown in Figure 10. It follows that the failure to induce an insulating state in GGA+U for $Ba_5Co_5FO_{13}$ is due most probably to the approximations made for the structure, namely, the structure $Ba_5Co_5FO_{13}$ used for calculations assumed the full occupation of the F site in its central position and chose one of the three split O3 positions leading to a very short F···O3 distance (i.e., 2.42 Å). This shows that the F-vacancies are crucial in governing the structure and properties. Nevertheless, the general features of the projected DOS plots obtained for $Ba_5Co_5O_{13}$ from GGA+U (with U = 1 eV) calculations are consistent with those obtained for $Ba_5Co_5FO_{13}$ from GGA calculations discussed in section 8.1. Several calculations carried out for 2H-$BaCoO_3$ with infinite chains of face-sharing octahedra showed also the difficulties of properly describing its electronic structure and the semiconducting behavior observed experimentally. In a recent study it has been shown that, in addition to the use of onsite repulsion U, the consideration of SOC is crucial in obtaining a band gap and properly describing its electronic structure.[28] Further studies including spin−orbit coupling would therefore be of great interest.

9. Spin Orientations

According to the electronic structure calculated for the model structures of $Ba_5Co_5F_{1-x}O_{13-\delta}$ presented in the previous section, it is reasonable to regard the Co_2O_7 tetrahedral dimers of

(27) Toulemonde, O.; Roussel, P.; Isnard, O.; André, G.; Mentré, O. *Chem. Mater.* **2010**. Submitted.

(28) Pardo, V.; Blaha, P.; Laskowski, R.; Baldomir, D.; Castro, J.; Schwarz, K.; Arias, J. E. *Phys. Rev. B* **2007**, *76*, 165120.

$Ba_5Co_5F_{1-x}O_{13-\delta}$ and $Ba_6Co_6F_{1-x}O_{16-\delta}$ as consisting of high-spin Co^{3+} (d^6) ions. Thus, the strong AFM coupling between the two Co sites in the Co_2O_7 tetrahedral dimers means that the magnetic orbitals of the two high-spin Co^{3+} (d^6) ions overlap substantially through the Co−O−Co superexchange path.[29] It is striking that the spins of the Co_2O_7 tetrahedral dimers are perpendicular to the *c*-direction in $Ba_5Co_5F_{1-x}O_{13-\delta}$ but parallel to the *c*-direction in $Ba_6Co_6F_{1-x}O_{16-\delta}$. It is important to check if this difference originates from the difference in the distortions in the Co_2O_7 tetrahedral dimers.

To probe this question, we consider the effect of SOC at the high-spin Co^{3+} (d^6) site by employing two independent coordinate systems for the orbital and spin angular momentum operators, e.g., (x, y, z) for $\hat{L}$ and (x', y', z') for $\hat{S}$. Provided that the z' axis of the spin (i.e., the preferred spin orientation) is specified by the polar angles θ and ϕ of the (x, y, z) coordinate system, the SOC Hamiltonian $\hat{H}_{SOC} = \lambda\hat{S}\cdot\hat{L}$ is written as[30,31]

$$\hat{H}_{SOC} = \lambda\hat{S}_{z'}\left(\hat{L}_z \cos\theta + \frac{1}{2}\hat{L}_+ e^{-i\phi}\sin\theta + \frac{1}{2}\hat{L}_- e^{i\phi}\sin\theta\right) + ... \quad (1)$$

where the spin-nonconserving term are omitted. With $\hat{H}_{SOC}$ as perturbation, the occupied d-states of a high-spin Co^{3+} site interact with the unoccupied d-states to lower the energy. The most important states for this energy lowering are those with the small energy gap Δe between them. Given the high-spin Co^{3+} (d^6) ion in each CoO_4 tetrahedron of the Co_2O_7 tetrahedral dimers (of $Ba_5Co_5F_{1-x}O_{13-\delta}$ and $Ba_6Co_6F_{1-x}O_{16-\delta}$), the small Δe occurs between the bottom three of the down-spin d-states. When these states (and their energies) are denoted by $\phi_1\downarrow$, $\phi_2\downarrow$, and $\phi_3\downarrow$ (e_1, e_2, and e_3), respectively (Figure 11), the stabilization energy ΔE induced by SOC is expressed as[30]

$$\Delta E = \frac{|\langle\phi_1\downarrow|\hat{H}_{SOC}|\phi_2\downarrow\rangle|^2}{\Delta e} - \frac{|\langle\phi_1\downarrow|\hat{H}_{SOC}|\phi_3\downarrow\rangle|^2}{\Delta e'} \quad (2)$$

where $\Delta e = e_2 - e_1$ and $\Delta e' = e_3 - e_1$. To see whether the stabilization energy ΔE prefers the $\|c$- or the $\perp c$-spin orientation, it is necessary to evaluate the $|\langle\phi_1\downarrow|\hat{H}_{SOC}|\phi_2\downarrow\rangle|^2$ and $|\langle\phi_1\downarrow|\hat{H}_{SOC}|\phi_3\downarrow\rangle|^2$ terms for $\theta = 0°$ (i.e., $\|c$) and $\theta = 90°$ (i.e., $\perp c$). In the present work we determine the molecular orbital MO's $\phi_1\downarrow$, $\phi_2\downarrow$, and $\phi_3\downarrow$ of the isolated CoO_4 tetrahedra, taken from the Co_2O_7 tetrahedral dimers of $Ba_5Co_5F_{1-x}O_{13-\delta}$ and $Ba_6Co_6F_{1-x}O_{16-\delta}$, by performing extended Hückel tight-binding (EHTB) calculations.[32] with the atomic parameters summarized in Table S10 (see the Supporting Information). The d-state split patterns obtained from EHTB calculations for the CoO_4 tetrahedra of the Co_2O_7 dimers found in $Ba_6Co_6F_{1-x}O_{16-\delta}$ and $Ba_5Co_5F_{1-x}O_{13-\delta}$ are presented in Figure 11a,b. Due to the distortions in the CoO_4 tetrahedra, the two-below-three split pattern expected for the d-states of T_d symmetry is missing, especially for the CoO_4 tetrahedron of $Ba_5Co_5F_{1-x}O_{13-\delta}$. As a result, it is difficult to characterize the orbital character of these d-states. Given that these states are occupied by a high-spin Co^{3+} (d^6) ion, the small energy gap between the occupied and unoccupied d-states occurs between the highest-occupied MO $\phi_1\downarrow$ and the lowest two unoccupied MOs $\phi_2\downarrow$ and $\phi_3\downarrow$. As a representative example, the shapes of the MOs $\phi_1\downarrow$, $\phi_2\downarrow$, and $\phi_3\downarrow$ calculated for an isolated CoO_4, taken from $Ba_5Co_5F_{1-x}O_{13-\delta}$, are shown in Figure 11, and the coefficients for their d-orbitals (i.e., $x^2 - y^2$, z^2, xy, xz, yz) are listed in Table 2a for the CoO_4 tetrahedron of $Ba_5Co_5F_{1-x}O_{13-\delta}$, and in Table 2b for that of $Ba_6Co_6F_{1-x}O_{16-\delta}$.

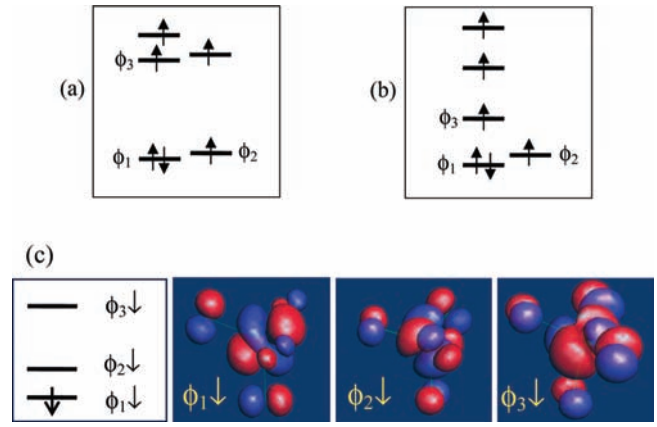

Figure 11. Split patterns of the d-block levels of the CoO_4 tetrahedra of the Co_2O_7 dimer found in (a) $Ba_6Co_6F_{1-x}O_{16-\delta}$ and (b) $Ba_5Co_5F_{1-x}O_{13-\delta}$, where the electron occupation assumed the presence of a high-spin Co^{3+} (d^6). (c) Shapes of the highest-occupied and the lowest two unoccupied down-spin MOs obtained for an isolated CoO_4 tetrahedron of the Co_2O_7 dimer found in $Ba_5Co_5F_{1-x}O_{13-\delta}$. These results were obtained from EHTB calculations.

Table 2. Coefficients for the d-Orbitals (i.e., $x^2 - y^2$, z^2, xy, xz, yz) Leading to the Highest-Occupied MO $\phi_1\downarrow$ and the Lowest Two Unoccupied MOs $\phi_2\downarrow$ and $\phi_3\downarrow$ of an Isolated CoO_4 Tetrahedron (taken from the Co_2O_7 tetrahedral dimer of $Ba_5Co_5F_{1-x}O_{13-\delta}$ and $Ba_6Co_6F_{1-x}O_{16-\delta}$) Obtained from EHTB Calculations

	$x^2 - y^2$	z^2	xy	xz	yz
(a) $Ba_5Co_5F_{1-x}O_{13-\delta}$					
$\phi_1\downarrow$	0.2504	0.4078	0.4344	−0.6077	−0.3498
$\phi_2\downarrow$	−0.4953	0.0000	−0.2848	0.3809	−0.6613
$\phi_3\downarrow$	−0.2614	0.7437	−0.4534	0.0535	0.0299
(b) $Ba_6Co_6F_{1-x}O_{16-\delta}$					
$\phi_1\downarrow$	0.2708	0.2020	0.4691	−0.6488	−0.3740
$\phi_2\downarrow$	0.4848	0.0000	−0.2792	0.3816	−0.6645
$\phi_3\downarrow$	−0.2754	0.6659	−0.4775	−0.1897	−0.1102

To evaluate the $|\langle\phi_1\downarrow|\hat{H}_{SOC}|\phi_2\downarrow\rangle|^2$ term, we note that the angular parts of the d-orbitals are expressed in terms of spherical harmonics as

$$\begin{aligned} x^2 - y^2 &\propto (Y_2^2 + Y_2^{-2})/\sqrt{2} \propto (|2,2\rangle + |2,-2\rangle)/\sqrt{2} \\ xy &\propto -i(Y_2^2 - Y_2^{-2})/\sqrt{2} \propto -i(|2,2\rangle - |2,-2\rangle)/\sqrt{2} \\ yz &\propto i(Y_2^1 + Y_2^{-1})/\sqrt{2} \propto i(|2,1\rangle + |2,-1\rangle)/\sqrt{2} \\ xz &\propto -(Y_2^1 - Y_2^{-1})/\sqrt{2} \propto -(|2,1\rangle - |2,-1\rangle)/\sqrt{2} \\ z^2 &\propto Y_2^0 \propto |2,0\rangle \end{aligned} \quad (3)$$

Therefore, given the following properties of the spherical harmonics,

(29) For reviews see: (a) Whangbo, M.-H.; Koo, H.-J.; Dai, D. *J. Solid State Chem.* **2003**, *176*, 417. (b) Whangbo, M.-H.; Dai, D.; Koo, H.-J. *Solid State Sci.* **2005**, *7*, 827.
(30) (a) Dai, D.; Xiang, H. J.; Whangbo, M.-H. *J. Comput. Chem.* **2008**, *29*, 2187. (b) Koo, H.-J.; Xiang, H. J.; Lee, C.; Whangbo, M.-H. *Inorg. Chem.* **2009**, *48*, 9051. (c) Xiang, H. J.; Wei, S.-H.; Whangbo, M.-H.; Da Silva, J. L. F. *Phys. Rev. Lett.* **2008**, *101*, 037209. (d) Xiang, H. J.; Wei, S.-H.; Whangbo, M.-H. *Phys. Rev. Lett.* **2008**, *100*, 167207. (e) Xiang, H. J.; Whangbo, M.-H. *Phys. Rev. B* **2007**, *75*, 052407.
(31) Wang, X.; Wu, R.; Wang, D.-S.; Freeman, A. J. *Phys. Rev. B* **1996**, *54*, 61.
(32) (a) Hoffmann, R. *J. Chem. Phys.* **1963**, *39*, 1397. (b) Our calculations were carried out by employing the SAMOA (Structure and Molecular Orbital Analyzer) program package. This program can be downloaded from the website, http://chvamw.chem.ncsu.edu/.

$$\begin{aligned}\hat{L}_z|L, L_z\rangle &= L_z|L, L_z\rangle \\ \hat{L}_+|L, L_z\rangle &= \sqrt{(L + L_z + 1)(L - L_z)}|L, L_z + 1\rangle \\ \hat{L}_-|L, L_z\rangle &= \sqrt{(L - L_z + 1)(L + L_z)}|L, L_z - 1\rangle\end{aligned} \quad (4)$$

we obtain for $\theta = 0°$

$$\begin{aligned}\langle xy|\hat{H}_{SOC}|x^2 - y^2\rangle &= \langle x^2 - y^2|\hat{H}_{SOC}|xy\rangle^* \propto 2i \\ \langle yz|\hat{H}_{SOC}|xz\rangle &= \langle xz|\hat{H}_{SOC}|yz\rangle^* \propto i\end{aligned} \quad (5)$$

and for $\theta = 90°$

$$\begin{aligned}\langle x^2 - y^2|\hat{H}_{SOC}|xz\rangle &\propto i \sin\phi \\ \langle x^2 - y^2|\hat{H}_{SOC}|yz\rangle &\propto i \cos\phi \\ \langle xy|\hat{H}_{SOC}|xz\rangle &\propto i \cos\phi \\ \langle xy|\hat{H}_{SOC}|yz\rangle &\propto -i \sin\phi \\ \langle xz|\hat{H}_{SOC}|z^2\rangle &\propto i\sqrt{3} \sin\phi \\ \langle yz|\hat{H}_{SOC}|z^2\rangle &\propto i\sqrt{3} \cos\phi\end{aligned} \quad (6)$$

All other matrix elements of $\hat{H}_{SOC}$ are zero. Table 3 summarizes the relative values of the $|\langle\phi_1\downarrow|\hat{H}_{SOC}|\phi_2\downarrow\rangle|^2$ and $|\langle\phi_1\downarrow|\hat{H}_{SOC}|\phi_3\downarrow\rangle|^2$ terms calculated for the $\|c$-spin orientation (i.e., $\theta = 0°$) and the $\perp c$-spin orientations ($\theta = 90°$, $\phi = 0°$ and $\theta = 90°$, $\phi = 90°$) for the CoO_4 tetrahedra of $Ba_5Co_5F_{1-x}O_{13-\delta}$ and $Ba_6Co_6F_{1-x}O_{16-\delta}$. For $Ba_5Co_5F_{1-x}O_{13-\delta}$, the $|\langle\phi_1\downarrow|\hat{H}_{SOC}|\phi_2\downarrow\rangle|^2$ term prefers the $//c$-spin orientation slightly, but the $|\langle\phi_1\downarrow|\hat{H}_{SOC}|\phi_3\downarrow\rangle|^2$ term strongly prefers the $\perp c$-spin orientation. For $Ba_6Co_6F_{1-x}O_{16-\delta}$, the $|\langle\phi_1\downarrow|\hat{H}_{SOC}|\phi_2\downarrow\rangle|^2$ term strongly prefers the $//c$-spin orientation, and the $|\langle\phi_1\downarrow|\hat{H}_{SOC}|\phi_3\downarrow\rangle|^2$ term strongly prefers the $\perp c$-spin orientation. Thus, the observed $\perp c$-spin orientation for $Ba_5Co_5F_{1-x}O_{13-\delta}$ is explained if the contribution of the $|\langle\phi_1\downarrow|\hat{H}_{SOC}|\phi_3\downarrow\rangle|^2$ term is substantial and the observed $//c$-spin orientation for $Ba_6Co_6F_{1-x}O_{16-\delta}$ if the contribution of the $|\langle\phi_1\downarrow|\hat{H}_{SOC}|\phi_3\downarrow\rangle|^2$ term is small. This is quite probable because the $\Delta e'/\Delta e$ ratio is considerably smaller for $Ba_5Co_5F_{1-x}O_{13-\delta}$ than for $Ba_6Co_6F_{1-x}O_{16-\delta}$. (Our EHTB calculations show that $\Delta e = 0.06$ eV and $\Delta e' = 0.36$ eV for $Ba_5Co_5F_{1-x}O_{13-\delta}$, and $\Delta e = 0.04$ eV and $\Delta e' = 0.58$ eV for $Ba_6Co_6F_{1-x}O_{16-\delta}$.) This result is consistent with experiment and confirms the indirect influence of the anionic vacancies on the final magnetic anisotropy.

10. Concluding Remarks

In this work, we investigated the effects of the anionic sublattice on the structures and magnetic properties in two oxyfluorides $Ba_5Co_5F_{0.77}O_{12.88}$ and $Ba_6Co_6F_{0.93}O_{16}$, which are insulating antiferromagnets. The fluorine vacancies present in the $[BaOF_{1-x}]$ layer are found to play a crucial role in distorting the tetrahedral dimers Co_2O_7, which arises from the off-centering of the O positions toward the vacant F positions.

Table 3. Values of the $|\langle\phi_1\downarrow|\hat{H}_{SOC}|\phi_2\downarrow\rangle|^2$ and $|\langle\phi_1\downarrow|\hat{H}_{SOC}|\phi_3\downarrow\rangle|^2$ Terms Calculated for the $\|c$ Orientation (i.e., $\theta = 0°$) and the $\perp c$ Orientations ($\theta = 90°$, $\phi = 0°$ and $\theta = 90°$, $\phi = 90°$) of the Spin in the CoO_4 Tetrahedron

		$\theta = 0°$	$\theta = 90°$, $\phi = 0°$	$\theta = 90°$, $\phi = 90°$
$Ba_5Co_5F_{1-x}O_{13-\delta}$	$\|\langle\phi_1\downarrow\|\hat{H}_{SOC}\|\phi_2\downarrow\rangle\|^2$	0.38	0.33	0.26
	$\|\langle\phi_1\downarrow\|\hat{H}_{SOC}\|\phi_3\downarrow\rangle\|^2$	0.10	0.29	0.67
$Ba_6Co_6F_{1-x}O_{16-\delta}$	$\|\langle\phi_1\downarrow\|\hat{H}_{SOC}\|\phi_2\downarrow\rangle\|^2$	0.44	0.18	0.23
	$\|\langle\phi_1\downarrow\|\hat{H}_{SOC}\|\phi_3\downarrow\rangle\|^2$	0.14	0.19	0.63

$Ba_5Co_5F_{0.77}O_{12.88}$ has more distorted Co_2O_7 dimers than does $Ba_6Co_6F_{0.93}O_{16}$, because it has more F vacancies. The local distortion of the Co_2O_7 dimers are responsible for the magneto−crystalline anisotropy, which leads to the spin orientation perpendicular to the *c*-axis in $Ba_5Co_5F_{0.77}O_{12.88}$ but parallel to the *c*-axis in $Ba_6Co_6F_{0.93}O_{16}$. This difference in the spin orientations of the two compounds, observed from our neutron diffraction experiments, arises from the fact that the distortions of the Co_2O_7 dimers in the two compounds are different. Our DFT calculations indicate that each Co(T_d) site has a high-spin Co^{3+} ion, and each Co(O_h) site a low-spin Co^{3+}/Co^{4+} ion. This description should be valid for other similar oxyhalides and $BaCoO_{3-\delta}$ polymorphs. It is encouraging that the difference in the spin orientations of the two closely related compounds $Ba_5Co_5F_{0.77}O_{12.88}$ and $Ba_6Co_6F_{0.93}O_{16}$ can be explained by considering SOC on the basis of the d-states of the distorted CoO_4 tetrahedra. This analysis for spin orientation would be of use for various magnetic compounds.

Acknowledgment. The work at NCSU was supported by the Office of Basic Energy Sciences, Division of Materials Sciences, U.S. Department of Energy, under Grant DE-FG02-86ER45259 and also by the resources of the HPC center of NCSU. The Laboratoire Léon Brillouin (Saclay, France) is thanked for providing neutron facilities. The USTL Centre de ressources informatiques (partially funded by "Fonds Européen de Développement Régional (FEDER)") for allocating CPU time. The "Fonds Européen de Développement Régional (FEDER)", "CNRS", "Région Nord Pas-de-Calais" and "Ministère de l'Education Nationale de l'Enseignement Supérieur et de la Recherche" are acknowledged for fundings of X-ray diffractometers. This work was carried out under the framework of the MAD-BLAST project supported by the ANR (grant No. ANR-09-BLAN-0187-01).

Supporting Information Available: Tables S1−S8 of the structural parameters from ND and from room-temperature and high-temperature single-crystal XRD. Figure S9 of the PND rietveld refinements. Table S10 of the atomic orbital parameters employed in the present EHTB calculations. This material is available free of charge via the Internet at http://pubs.acs.org.

JA100170M